Water Science & Technology

Water Science & Technology Vol 87 No 1, 284 doi: 10.2166/wst.2022.428

Adsorptive removal of pharmaceutically active compounds from multicomponent system using *Azadirachta indica* induced zinc oxide nanoparticles: analysis of competitive and cooperative adsorption

Nayanathara O. Sanjeev [a,*], Manjunath Singanodi Vallabha[b] and Aswathy E Valsan[a]

[a] Department of Civil Engineering, National Institute of Technology, Calicut, Kerala, India
[b] Department of Civil Engineering, B.M.S. College of Engineering, Bangalore, Karnataka 560019, India
*Corresponding author. E-mail: nayanatharaos92@gmail.com

NOS, 0000-0001-9939-4676

ABSTRACT

In this research, zinc oxide (ZnO) nanoparticles synthesized using neem leaf (*Azadirachta indica*) extract were used as an adsorbent for removing two widely used pharmaceutical compounds acetaminophen (AMP) and sulfadiazine (SDZ). The synthesized ZnO nanoparticles were characterized using SEM-EDS, FTIR, TEM, BET, and XRD analysis. The synthesized ZnO nanoparticles were found to be in the size range of 10 nm with a surface area of 48.551 m^2/g. The adsorptive performance of ZnO nanoparticles in both mono-component (MoS) and multi-component system (MuS) was investigated under various operational parameters viz. contact time, temperature, pH, concentration of pharmaceutical compound and ZnO nanoparticles dose. It was observed that the maximum adsorption capacity of ZnO nanoparticles was 7.87 mg/g and 7.77 mg/g for AMP and SDZ, respectively, under the optimum conditions of 7 pH and 2 g/L adsorbent dosage. The experimental data best-fitted with the pseudo-second-order model and Langmuir model, indicating monolayer chemisorption. Further investigation on removal of AMP and SDZ from multicomponent system was modelled using a Langmuir competitive model. The desorption study has shown 25.28% and 22.4% removal of AMP and SDZ from the surface of ZnO nanoparticles. In general, green synthesized ZnO nanoparticles can be utilized effectively as adsorbent for removal of pharmaceutically active compounds from wastewater.

Key words: acetaminophen, adsorption, competitive adsorption, green synthesis, sulfadiazine, zinc oxide nanoparticle

HIGHLIGHTS

- Zinc oxide nanoparticles were synthesized from *Azadirachta indica* leaf extract.
- Removal of pharmaceutically active compounds sulfadiazine and acetaminophen using ZnO nanoparticles was investigated in a mono-component and multi-component system.
- An adsorption study in a multi-component system was performed using Langmuir's competitive model and nature of adsorption was studied.
- Recyclability of the adsorbent was studied.

GRAPHICAL ABSTRACT

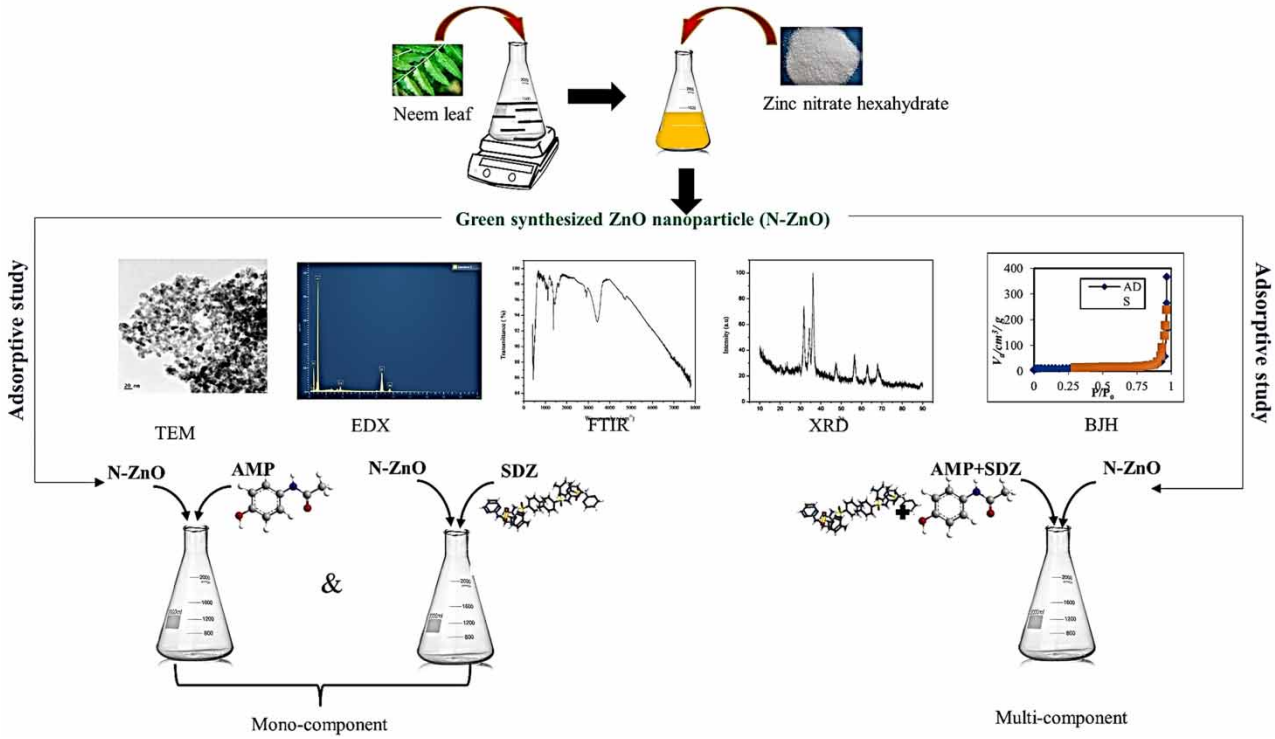

1. INTRODUCTION

Emerging contaminants (ECs) are the micro-pollutants present in the aqueous environment that do not have any discharge standards and are not monitored stringently (Taheran *et al.* 2018). The sources of ECs in the aqueous environment include the discharge of effluents from various industries such as pharmaceuticals, animal husbandry, poultry, aquaculture and wastewater from septic tanks of residential buildings (Thomaidis *et al.* 2012). The persistence and detrimental effects of ECs are recently a problem of rising concern across the world (Natarajan *et al.* 2021). These compounds are seldom removed in the conventional treatment process and require high end treatment method for their efficient removal (Gomes *et al.* 2020). As a result, they finally reach surface or groundwater bodies by infiltration, surface runoff etc. resulting in its contamination.

Pharmaceutically active compounds (PACs) such as hormones, stimulants, analgesic, antiepileptics, antibiotics, β-blockers etc., are an important category of ECs. The PACs from hospital effluent, animal husbandry, domestic sewage and pharmaceutical manufacturing industries are the main source of pharmaceutical contamination in aquatic ecosystem (Sim *et al.* 2011). Currently, more than hundreds of tonnes of PACs are produced annually and about 3,000 of them are used as medicines (Sim *et al.* 2011). Over the past few decades, the unrestricted use of PACs has led to the pollution of aquatic ecosystems. The consumption of PACs has increased by around 2.8 times over a span of 15 years resulting in an increase in revenue from US$390.2 billion (2001) to US$1,105.2 billion (2016).

Among the different ECs, sulfadiazine (SDZ) and acetaminophen (AMP) are the most extensively used antibacterial (Xu *et al.* 2013) and antipyretic drugs (Briones *et al.* 2014), respectively. In most of the developing countries, the intake of AMP is without any medical prescription and ~58–68% of the AMP consumed finds its way into wastewater streams through urine and excreta (Ahmadzadeh & Dolatabadi 2018). In India AMP is identified as one of the most critical compounds for further treatment and monitoring (Chinnaiyan & Thampi 2018) and is largely detected in sewage treatment plants (Subedi *et al.* 2017), surface water bodies (Mutiyar *et al.* 2018; Kumar *et al.* 2019), etc. The presence of SDZ has also been reported in various environmental compartments like groundwater and river water, livestock farms, and wastewater treatment plant (Baran *et al.* 2011; Liu *et al.* 2018). Notably, AMP and SDZ can degrade and transform into different metabolites, of which some of them (e.g., benzoquinone and hydroquinone) are noxious to other life forms and humans (Yang *et al.* 2018; Phong Vo

et al. 2019). It is essential to prevent these pharmaceutical compounds from reaching aqueous environments since they can lead to ecotoxicity through bio-accumulation and bio-magnification.

Various authors have investigated different methods for removing AMP and SDZ from aqueous media including physico-chemical and biological processes involving membrane technology, advanced oxidation, adsorption etc. (Phong Vo *et al.* 2019; Li *et al.* 2020; Yadav *et al.* 2022). In comparison to other technologies, adsorption is one of the effective and efficient technique for removal of ECs from wastewater owing to its low-cost installation, no sludge formation, simple operational design and easy maintenance (Liu *et al.* 2015). Activated carbon and its modified forms are the most commonly used adsorbent for removal of micropollutants (Phong Vo *et al.* 2019). Some examples of modified forms include granular type, chitosan-nano and phosphoric acid-modified activated carbon (Amouzgar *et al.* 2017; Wong *et al.* 2018; Yanyan *et al.* 2018). Lately, nano-particles are gaining wide popularity as adsorbents for removal of micro pollutants involving pharmaceutically active compounds from effluents owing to their higher surface area and excellent adsorption properties (He *et al.* 2021; Rathi & Kumar 2021).

Zinc oxide (ZnO) nanoparticles exhibit properties like thermal and chemical stability, high adsorptive nature towards inorganic and organic pollutants in the aqueous matrix, high surface area and photon absorption efficiency, non-toxicity, availability and cost effectiveness (Wong *et al.* 2018). Methods for synthesising ZnO nanoparticles includes sol-gel method (Al Abdullah *et al.* 2017), hydrothermal and (Aneesh *et al.* 2007) and precipitation method (Ghorbani *et al.* 2015). The major drawbacks associated with these methods are release of toxic chemicals (Sangeetha *et al.* 2011) and requirement of sophisticated conditions involving high temperature and pressure, resulting in increased energy consumption (Hassan *et al.* 2016).

Green synthesis of ZnO nanoparticles is gaining wide popularity nowadays due to its inherent advantages namely low cost, eco-friendly, and non-toxic chemicals (Moritz & Geszke-Moritz 2013). Several authors have synthesized ZnO nanoparticles using the extracts from different plants such as *Aloe vera* (Ali *et al.* 2016), *Hibiscus subdariffa* (Bala *et al.* 2014), *Aloe barbadensis miller* (Sangeetha *et al.* 2011), *Azadirachta indica* (Bhuyan *et al.* 2015; Madan *et al.* 2015; Mankad *et al.* 2016), *Moringa olifera* (Matinise *et al.* 2017) etc. The ZnO nanoparticles synthesized via green method (from different sources) can be used effectively for removing heavy metals (Angelin *et al.* 2015; Moustafa Ahmed P & Yousef 2015; Anusa *et al.* 2017; Azizi *et al.* 2017; Yuvaraja *et al.* 2018).

Azadirachta indica, popularly known as neem, is common to India and other southeast countries. It belongs to the Meliaceae family, and has been used widely in the Ayurvedic treatment for more than 4,000 years due to its excellent medicinal property (Pandey *et al.* 2014). Neem leaf extract was found to exhibit antimicrobial property against several fungal and bacterial strains (Ali *et al.* 2021). In this research, neem leaf is selected for synthesizing ZnO nanoparticles, as the neem leaf extract is rich in phytochemicals like alkaloids, flavonoids, steroids, carbohydrates, terpenoids and glycosides compounds (Bhuyan *et al.* 2015). These compounds function as bio-reductant which take part in the conversion of zinc ions to ZnO nanoparticles. Furthermore, the neem leaf extract also functions as capping and stabilizing agent, thereby eliminating the need for additional toxic chemicals during the synthesis process (Bhuyan *et al.* 2015).

Majority of previously reported studies have determined the adsorption of pharmaceutically active compounds from mono-component systems. Meanwhile, simultaneous removal of pharmaceutically active compounds from mono and multicomponent system has been less explored. The removal of AMP and SDZ from mono-component (MoS) and multi-component systems (MuS) using green synthesized ZnO nanoparticles has not been widely investigated. A proper knowledge of the effect of one PAC in the presence of another, i.e., cooperative adsorption (synergistic adsorption) or competitive adsorption (antagonistic adsorption) is not elucidated. It is also important to identify the antagonistic or/and synergistic effect of different PACs present in multicomponent systems. The equilibrium of multicomponent systems represented using multicomponent models is rarely addressed in literatures. Hence, it is intended to perform the sorptive removal of pharmaceutically active compounds of different classes from multi-component systems using green synthesized ZnO nanoparticles.

Green synthesized ZnO nanoparticles from neem leaf (*A. indica)* extract for removal of AMP and SDZ from the MoS (AMP/SDZ) and the MuS (AMP + SDZ) will be investigated in this research. The scope of this research includes (a) green synthesis of ZnO nanoparticles from the leaf extract of *A. indica*, characterizing using SEM-EDS, TEM, FTIR, BET, XRD and applying for removal of AMP and SDZ; (b) perform analysis of various kinetic and isotherm models to determine the rate constant, maximum adsorption capacity, and sorption mechanism; (c) assess the MuS with the help of competitive Langmuir model for examining the synergistic and antagonistic nature of adsorption for removal of SDZ and AMP; (d) perform a

desorption study to check the reusability and recovery of ZnO nanoparticles and (e) performance evaluation of adsorption capacity of synthesized ZnO nanoparticles with other green synthesized ZnO nanoparticles from literature.

2. MATERIALS AND METHODS

2.1. Materials

The fresh leaves of *A. indica* (neem tree) were collected from the campus of National Institute of Technology in Calicut, India for synthesizing the adsorbent. Zinc nitrate hexahydrate of analytical grade and 96% purity was purchased from Merck (Chemind, Calicut, India). AMP and SDZ standards of analytical grade and 99.9% purity was procured from Sigma Aldrich. Water, phosphate buffer, acetonitrile, and methanol used for the study were of analytical grade.

2.2. Synthesis of N-ZnO nanoparticles

There are different methods for the synthesis of ZnO nanoparticles using *A. indica* (Mankad *et al.* 2016; Bhuyan *et al.* 2015; Madan *et al.* 2015). However, in this study, the synthesis of ZnO nanoparticles from *A. indica* leaf extract was performed by slightly modifying the procedure followed by Elumalai & Velmurugan (2015). The procedure for ZnO nanoparticles synthesis from neem leaf is depicted in Figure 1. Freshly collected neem leaves were washed using tap water initially, followed by distilled water to remove other impurities and dust. The washed leaves were kept for drying at room temperature and 20 g of neem leaf was allowed to boil in 100 mL distilled water for 10 minutes. The extract was filtered using Whatman 41 filter paper after cooling and 20 mL of the filtered extract was added with 2 g of zinc nitrate hexahydrate under continuous stirring at 1,500 rpm and heated to a temperature of around 60–80 °C until a thick yellow colour paste is obtained. The obtained paste was then collected to a crucible and was heated in a muffle furnace for 2 hours at 400 °C. A white-coloured powder obtained at the end is stored and used as an adsorbent ZnO nanoparticle for the removal of AMP and SDZ.

2.3. Characterization of ZnO nanoparticles

The synthesized ZnO nanoparticles was characterized using SEM, EDS, BET, FTIR and XRD techniques. Fourier-transform infrared spectroscopy (FTIR) analysis was performed to identify the functional groups present on the surface of ZnO nanoparticles (Jasco FTIR-4700, frequency range 400–8,000 cm^{-1}). Meanwhile, the crystallinity of N-ZnO was examined using XRD analysis (X'Pert^3 Powder, PANalytical). Subsequently, surface morphology and elemental composition was investigated by scanning electron microscopy equipped with energy dispersive spectroscopy (SEM-EDS) (FEI- Quanta 200, operating voltage 15 kV). Transmission electron microscopy (TEM) (JEOL JEM 2100, LaB6 Type, operating voltage 200 kV) analysis was performed to understand the size of the nanoparticles. The surface area of the samples was analyzed using Brunauer–Emmett–Teller (BET) analysis (Belsorp, passing nitrogen gas at 77 K).

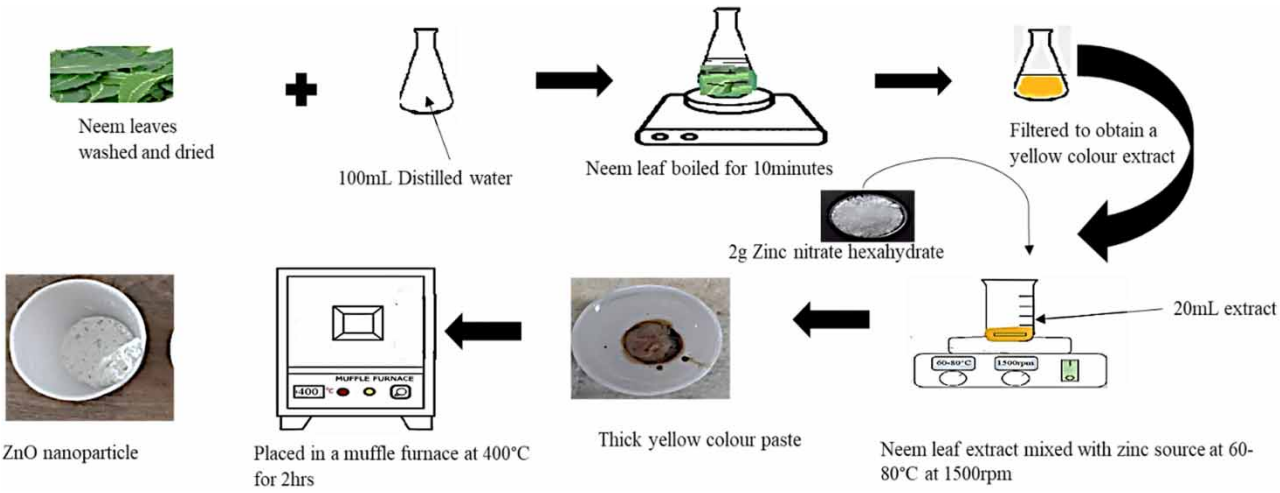

Figure 1 | Green synthesis of ZnO nanoparticles adsorbent from neem leaf extract.

2.4. Quantification of SDZ and AMP

The AMP and SDZ procured from Sigma Aldrich is pharmaceutical secondary standard: certified reference material of 99.9% purity. Removal of AMP and SDZ was determined with the help of high-performance liquid chromatography (HPLC) (HPLCDGU-14A degasser model, Shimadzu LC-20AD pump, SPD-M20APDA detector) coupled with C18 analytical column at a flowrate of 1 mL/min. The concentration of AMP was determined using acetonitrile and phosphate buffer in the volume ratio of 40:60 at 254 nm. On the other hand, SDZ samples were quantified using water and methanol in the volume ratio of 40:60 at 263 nm. Since no recovery study was performed, to check the accuracy of the data, initially sample was run with HPLC water alone. This was followed by spiking water with 25 mg/L, 50 mg/L and 100 mg/L of AMP and SDZ respectively. For both AMP and SDZ no peak was detected for distilled water. However, sharp peak was detected at 3.4 minutes for AMP and at 4.2 minutes for SDZ respectively at all concentrations.

This was followed by preparing the stock solutions containing 1 g/L of either SDZ or AMP by solubilizing 1 g of AMP/SDZ in 1 L of distilled water. The prepared stock solution was diluted further to obtain the working solutions of different concentrations (5, 10, 25, 50, 75 and 100 mg/L). The prepared SDZ and AMP solutions were analyzed using HPLC. From the standard solutions of different concentration, a calibration curve was plotted for both AMP and SDZ. The R^2 value was found to be 0.997 for AMP and 0.993 for SDZ respectively.

2.5. Experimental methodology

2.5.1. Mono-component system (MoS)

The adsorption experiments were carried out using an accurately weighed quantity of ZnO nanoparticles added to 25 mL AMP/SDZ solution in 100 mL conical flasks. This sorbent-sorbate mixture was kept at 200 rpm in a shaking incubator for 45 min at 30 °C. The experiments were performed by varying the solution pH (2–12), contact time (5–45 min), initial AMP/SDZ concentration (0.5–100 mg/L) and ZnO nanoparticles dosage (0.2–4 g/L). Subsequently, an aliquot of samples was collected at frequent time intervals and analyzed for determining the concentration of AMP and SDZ. The percentage removal of AMP and SDZ was calculated using Equation (1).

$$Removal\ (\%) = \frac{(C_i - C_t)}{C_i} \times 100 \tag{1}$$

where, C_i and C_t indicates the concentration of target pollutants at beginning and at any time 't', respectively.

The equilibrium adsorption capacity (q_e) of green synthesized nanoparticles for removal of AMP and SDZ was determined using Equation (2).

$$q_e \left(\frac{mg}{g}\right) = \frac{(Co - Ce)}{m} \times V \tag{2}$$

where, m is the mass of the adsorbent (g) and V is the volume of pharmaceutical solution (L).

2.5.2. Multi-component system (MuS)

Similar to MoS, MuS adsorption experiments were performed in batch mode using a 100 mL Erlenmeyer flask and at a temperature of 30 °C. About 25 mL of the mixture of AMP + SDZ (mixed at different proportions) solution was kept at 200 rpm in a shaking incubator. The proportions of SDZ and AMP in the SDZ + AMP mixture were taken as 1 + 1, 5 + 5, 10 + 10, 25 + 25, 50 + 50 and 100 + 100 mg/L. The optimum dose obtained from the MoS study was added to the AMP + SDZ mixture. To study the adsorption in a MuS, the competitive Langmuir isotherm was adopted to model the AMP + SDZ mixture (Manjunath & Kumar 2018). Equations (3) and (4) represent the Langmuir model for MoS and MuS, respectively.

$$q_e = \frac{q_m K_L C_e}{1 + K_L C_e} \tag{3}$$

$$q_{e,ij} = \frac{q_m K_{L,ij} C_{e,ij}}{1 + \sum K_{L,ij} C_{e,ij}} \tag{4}$$

Where, q_e and q_m are equilibrium and maximum adsorption capacity, respectively (mg/g), K_L indicates Langmuir equilibrium constant, and C_e indicates target pollutants concentration at equilibrium (mg/L).

2.6. Kinetics study

A batch adsorption study was performed under a pH of 7 and an initial AMP/SDZ concentration of 5 mg/L for an optimum contact time. ZnO nanoparticles were added to the solution at a predetermined dose. The samples were collected at 5, 10, 15, 30, and 45 minutes. The experimental data was modelled using different kinetic models viz. pseudo-first-order (PFO), pseudo-second-order (PSO), intraparticle diffusion model (IDM), Elovich kinetic model (EKM), and liquid film diffusion model (LFD) to determine the kinetic constants (Akbour *et al.* 2020; Titchou *et al.* 2020, 2021).

2.7. Equilibrium study

Equilibrium study was performed to check the pertinence of the isotherm models (Mall *et al.* 2006; Akbour *et al.* 2020; Gaayda *et al.* 2022), which include Freundlich (FI), Langmuir (LI), Dubinin–Radushkevich (DRI), Elovich (EI), and Temkin (TI), under specified conditions such as pH of 7, optimum contact time, ZnO nanoparticles dosage and AMP/SDZ concentration in the range of 0.5, 1, 5, 10, 25, 50, 75 and 100 mg/L at 30 °C. Table 1 presents the expressions of various kinetic and isotherm models adopted for the removal of AMP and SDZ using ZnO nanoparticles.

2.8. Thermodynamic study

The nature of adsorption was evaluated from the thermodynamic viewpoint. This was performed by varying the temperature in the range of 20 °C, 25 °C, 30 °C and 35 °C respectively at optimum adsorbent dosage and contact time. The standard values of enthalpy (ΔH°, kJ/mol), Gibbs free energy (ΔG°, kJ/mol) and entropy (ΔS°, J/mol/K) from the Equation (5).

$$\Delta G^{\circ} = -RT\ln K_d \tag{5}$$

where, ΔG° represents the standard Gibbs free energy change, T is the absolute temperature (°K), R is the universal gas

Table 1 | Adsorption models for removal of AMP and SDZ using ZnO nanoparticles

Type	Model	Expression	References
Kinetic	Pseudo-first-order	$\ln(q_e - q_t) = lnq_e - K_1 t$	Titchou *et al.* (2020)
	Pseudo-second-order	$\frac{t}{q_t} = \frac{1}{K_2 q_e^2} + \frac{t}{q_e}$	Akbour *et al.* (2020)
	Intra particle diffusion	$q_t = K_{ID} t^{1/2} + C$	Zhang *et al.* (2017)
	Liquid film diffusion	$ln\left(1 - \frac{q_e}{q_t}\right) = -K_{FD}\, t + A$	Manjunath *et al.* (2020)
	Elovich kinetic model	$q_t = \frac{1}{\beta} ln\alpha\beta + \frac{1}{\beta}\ln t$	Yadav *et al.* (2022)
Isotherm	Langmuir	$\frac{1}{q_e} = \frac{1}{q_m} + \frac{1}{q_m K_L C_e}$	Gaayda *et al.* (2022)
	Freundlich	$lnq_e = \ln K_F + \frac{1}{n} lnC_e$	Manjunath *et al.* (2019)
	Temkin	$q_e = BlnA_T + BlnC_e$	Titchou *et al.* (2021)
	Dubinin – Radushkevich	$lnq_e = \ln(q_m) - (K_{DR}\varepsilon^2)$	Manjunath & Kumar (2018)
	Elovich	$ln\frac{q_e}{C_e} = lnK_E q_m - \frac{1}{q_m} q_e$	Yadav *et al.* (2022)

Where,

Kinetic constants: q_e is equilibrium adsorption capacity (mg/g); q_t is adsorption capacity at time 't' (mg/g); K_1 is pseudo – first order rate constant (min – 1); K_2 is pseudo – second order rate constant (g/mg/min); K_{ID} is instra – particle diffusion rate constant (mg/g/min$^{0.5}$) and C is intercept; K_{FD} is iLiquid film diffusion rate constant (1/min), A is Liquid file constant; α and β are Elovich kinetic model constants; K_o and α are Bangham constants; m is mass of adsorbent and V is the volume of adsorbate sample.

Isotherm constants: q_e is equilibrium adsorption capacity (mg/g); q_m is maximum adsorption capacity (mg/g); K_L is Langmuir constant (L/mg); C_e is equilibrium concentration (mg/L); K_F and n are Freundlich constants; A_T is Temkin equilibrium constant (L/mg) and B is Temkin constant; K_{DR} is mean free energy of adsorption (mol^2/kJ^2) and $\varepsilon = RT\ln[1 + (1/C_e)]$ is Polyani potential; K_E is Elovich equilibrium constant (L/mg).

constant (8.314 J/mol K) and K_d represents the distribution coefficient. The value of K_d is determined from Equation (6) (Akbour *et al.* 2020).

$$\ln K_d = \frac{-\Delta H^o}{RT} + \frac{\Delta S^o}{R} \tag{6}$$

The change in enthalpy and entropy was determined from the linear plot connecting ln K_d vs 1/T. (Titchou *et al.* 2021). The change in free energy, entropy and enthalpy helps to understand the spontaneity, randomness and heat change in the adsorption of AMP and SDZ onto the surface of the ZnO nanoparticles (Manjunath & Kumar 2018).

2.9. Regeneration and reusability of ZnO nanoparticles

After the adsorption experiments, from the conical flasks containing the adsorbent ZnO nanoparticles, the supernatant AMP/SDZ solution was replaced with same volume of distilled water. The conical flasks with the ZnO nanoparticles-distilled water mixture is then mixed for 6 h at 30 °C in a shaking incubator. Samples were collected at an interval of 2 h. Adsorption-desorption studies were performed for three cycles to evaluate the percentage of sorbates desorbed from the surface of ZnO nanoparticles (Saranya *et al.* 2018). The desorption efficiency was determined using Equation (7).

$$Desorption\ (\%) = \frac{C_d}{C_a} \times 100 \tag{7}$$

where, C_a is AMP/SDZ adsorbed on the ZnO nanoparticles at time of equilibrium (mg/L) and C_d is AMP/SDZ desorbed from the surface of the ZnO nanoparticles (mg/L).

3. RESULTS AND DISCUSSION

3.1. Characterization of green synthesized ZnO nanoparticles

Figure 2(a)–2(f) depicts the characterization of green synthesized ZnO nanoparticles. Figure 2(a) shows the SEM image of ZnO nanoparticles synthesized from neem leaf extract. The image shows that the ZnO nanoparticles are spherical and well distributed. From figure, the surface pores that helps in sorption of AMP and SDZ are visible. From the TEM image (Figure 2(b)), the average particle size was approximately 10 nm. However, aggregations of particles are observed, which may be attributed to the densification of particles leaving behind narrow space between them and the high surface energy that usually happens when nanoparticles are synthesized in an aqueous medium (Elumalai & Velmurugan 2015). Meanwhile, the elements present in the nanoparticle were examined using EDS analysis as shown in Figure 2(c). It depicts the presence of zinc (74.95 wt%) and oxygen (22.66 wt%). In addition to Zn and O, Ca (2.39 wt%) was also seen in the EDS spectrum. This is due to the element Ca present in the natural composition of *A. indica* (Sahito *et al.* 2003). FTIR helps in identifying the functional groups of the ZnO. Figure 2(d) represents the FTIR spectrum of the synthesized adsorbent. The peak between 400 and 600 cm^{-1} indicates the vibrations of the zinc and oxygen bond (Varadavenkatesan *et al.* 2019). The cliffs at 922, 1,393, and 3,451 cm^{-1} depicts O-H bonds presence (Sangeetha *et al.* 2011). The peaks at 2,987 cm^{-1} represent the stretching vibration of amide II, amide linkage between the amino acid residues present in the proteins, and the evidence of atmospheric CO_2 (Bhuyan *et al.* 2015). However, on the surface of ZnO nanoparticles, some proteins, phenolic compounds, and terpenoids originating from plant extract can be identified. The carboxylic and free amino groups from these phytochemicals are responsible for the stability of the ZnO nanoparticles. The amide bands originating from proteins and the bonds -C-O-C-, -C = C- and -C-O- derived from heterocyclic compounds act as capping agents (Sangeetha *et al.* 2011). The XRD results of the ZnO nanoparticles (Figure 2(e)) marks the presence of well-defined diffraction peaks at 68.86°, 63.81°, 57.69°, 48.38°, 37.22°, 35.36°, and 32.72°, and denoting to (112), (103), (110), (102), (101), (002) and (100) respectively. This matches the standard JCPDS card No.89-0510 depicting ZnO nanoparticles' hexagonal wurtzite crystal structure (Varadavenkatesan *et al.* 2019). On the other hand, the BET adsorption-desorption isotherm for determining the surface area, pore size and pore volume of the ZnO nanoparticles is depicted in Figure 2(f). Since adsorption is a surface phenomenon, surface area of the adsorbent plays a critical role in the removal of target pollutants. The specific surface area obtained for ZnO nanoparticles was found to be 48.551 m^2/g. The average pore diameter was found to be 46.843 nm, which indicates the presence of mesopores. Pore volume also impart a vital role in adsorption process. The pore volume for N-ZnO was found to be 0.5686 cm^3/g. The specific surface area obtained from

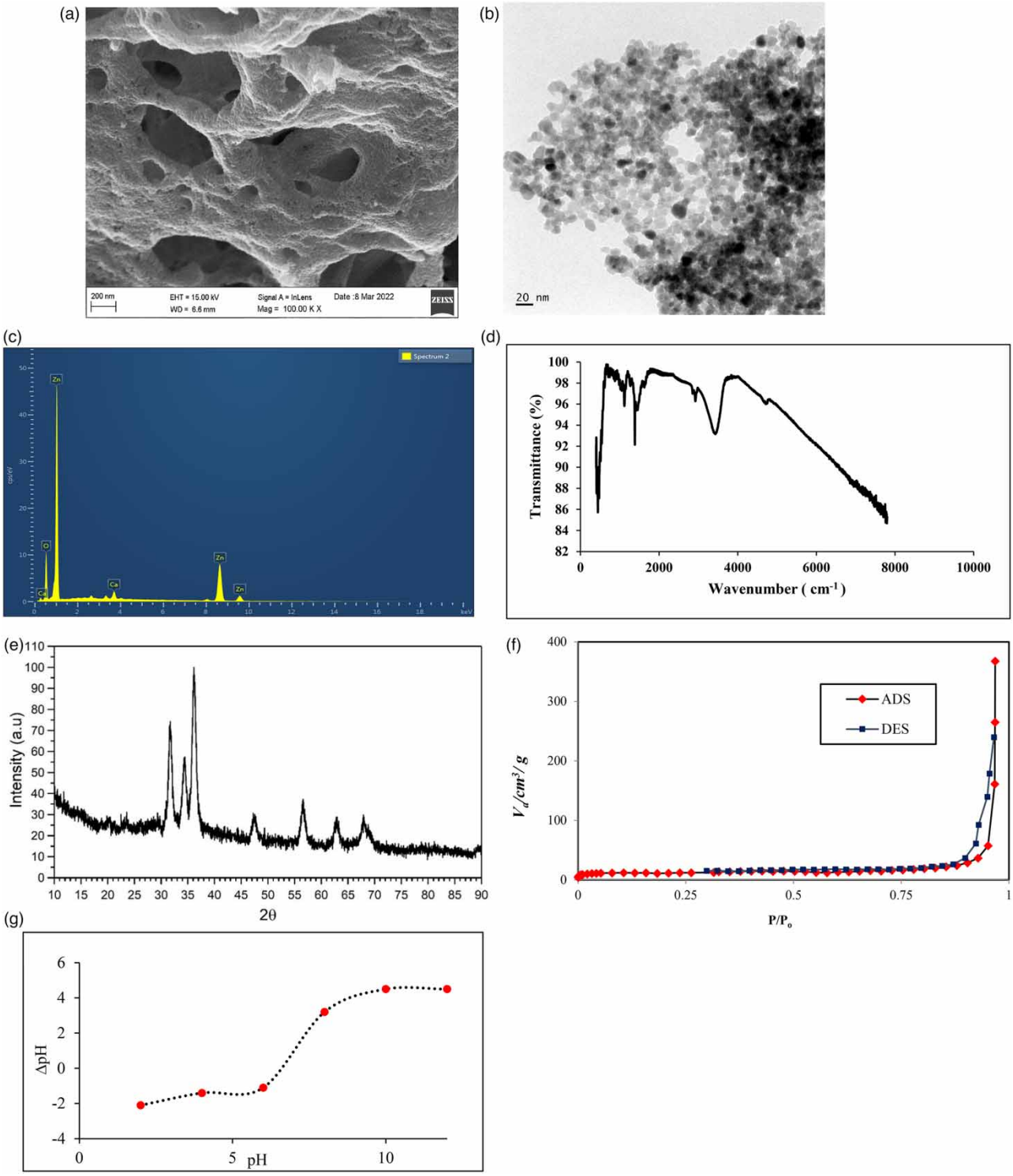

Figure 2 | Characterization of ZnO nanoparticles: (a) SEM, (b) TEM, (c) EDS, (d) FTIR, (e) XRD, (f) BJH plot and (g) pH_{pzc} analysis.

this study is higher when compared with other adsorbents synthesized using various sources as shown in Table 2. Furthermore, Figure 2(g) shows the pH_{pzc} (pH at point of zero charge) plot of synthesized ZnO nanoparticles and the value of pH_{pzc} of ZnO nanoparticles was observed to be 6.6. The pHsolution < pHpzc, specifies the surface of adsorbent N-ZnO as deprotonated

(negatively charged) and pHsolution > pHpzc, indicates that the surface of ZnO nanoparticles are in protonated form (positively charged).

3.2. Effect of operational parameters

The effect of operation parameters viz. contact time, ZnO nanoparticles dose, AMP/SDZ concentration, solution pH and temperature on removal of AMP and SDZ have been investigated.

3.2.1. Effect of contact time

The variation of removal with respect to contact time was studied at neutral pH for optimum adsorbent dose and target pollutants concentration 5 mg/L. Figure 3(a) shows the effect of contact time on removal of AMP and SDZ using N-ZnO nanoparticles. From figure it can be observed that the initial stages of adsorption till 5 min was found to be rapid, probably due to large concentration gradient between the solute adsorbed on the sorbent and the aqueous solute (Xu *et al.* 2013) along with the presence of a large number of active sites on the surface of ZnO nanoparticles (Wang *et al.* 2013). However, as time progresses, the rate of adsorption decreases as the vacant active sites get occupied by sorbate molecules and reaches equilibrium (Dutta *et al.* 2015). A maximum removal of 64.12% and 59.97% for AMP and SDZ, respectively, was observed at the end of 30 minutes which was taken as the equilibrium time. A similar trend in removal with respect to contact time was

Table 2 | Maximum BET area of green synthesized ZnO nanoparticles

Source of feedstock	BET surface area (m^2/g)	References
Ocimum sanctum	32.72	Nayak *et al.* (2020)
Apple-derived compounds	17.00	Soliman *et al.* (2020)
Peltophorum pterocarpum	13.56	Pai *et al.* (2019)
Calliandra haematocephala	9.18	Vinayagam *et al.* (2020)
Peltophorum pterocarpum pod extract	19.61	Vinayagam *et al.* (2021)
Cyanometra ramiflora	16.27	Varadavenkatesan *et al.* (2019)
Ocimum tenuiflorum	21.20	Dayakar *et al.* (2017)
Padina tetrastromatica	27.37	Pandimurugan & Thambidurai (2016)
Azadirachta indica	48.55	Present study

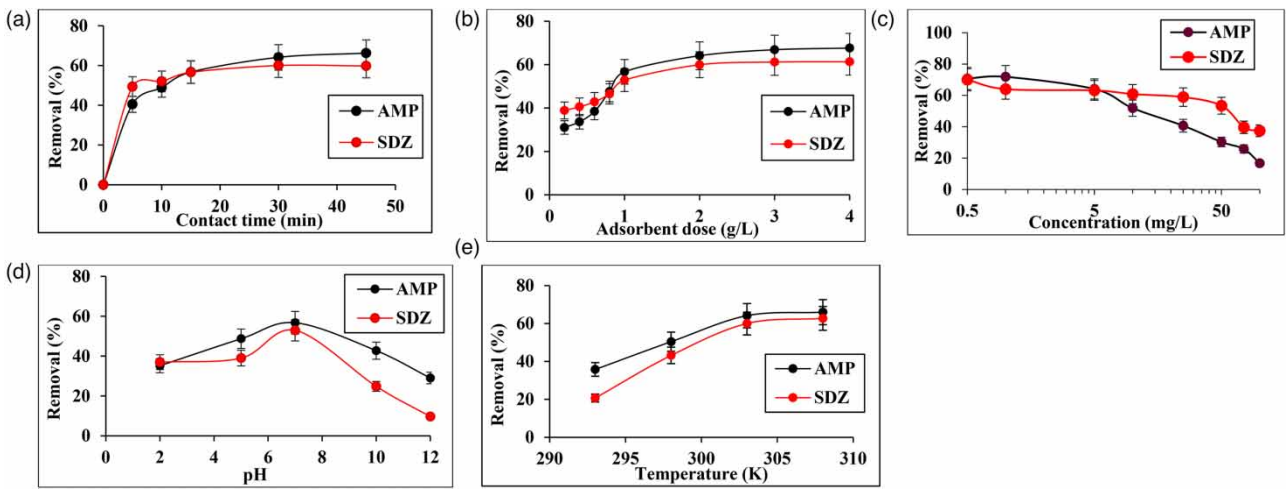

Figure 3 | Effect of operational parameters on removal efficiency (a) contact time (b) adsorbent dosage (c) Initial adsorbate concentration (d) pH (e) Temperature. *Note*: Experimental conditions: (a) t: 0–45 min, pH:7, ZnO nanoparticles dose: 2 g/L, SDZ/AMP conc: 5 mg/L, (b) N-ZnO dose (0.2–4 g/L), t: 30 min, pH:7, SDZ/AMP conc: 5 mg/L, (c) SDZ/AMP conc: 0.5–100 mg/L, ZnO nanoparticles dose: 2 g/L, t: 30 min, pH:7, (d) pH:2–12, SDZ/AMP conc: 5 mg/L, ZnO nanoparticles dose: 2 g/L, t: 30 min (e) Temp: 293–308 K, pH: 7, N-ZnO dose: 2 g/L, t: 30 min, SDZ/AMP conc: 5 mg/L.

observed for the removal of AMP using double oxidized graphene oxide, tea waste-derived activated carbon, and nano-silica and for the adsorptive removal of SDZ using spent tea waste derived chemically modified activated carbon (Dutta *et al.* 2015; Moussavi *et al.* 2016; Eslami *et al.* 2020; Yadav *et al.* 2022).

3.2.2. Effect of adsorbent dosage

The effect of ZnO nanoparticles dosage on the adsorption of AMP/SDZ was assessed at neutral pH, for an initial AMP/SDZ concentration of 5 mg/L and at contact 30 min. The result of the study is shown in Figure 3(b). From figure, it can be seen that increase in ZnO nanoparticles dose from 0.2 to 4 g/L showed increase in removal from 38.88% to 61.34% for SDZ and from 31.04% to 67.66% for AMP, respectively. This improvement in the removal with increase in ZnO nanoparticles dosage is mainly attributed to the increment in the number of available sites on the ZnO nanoparticles surface to contact with the fixed range of AMP/SDZ molecules (Moussavi *et al.* 2016). From the figure it can be seen that, for both SDZ and AMP, at a dose >2 g/L, there was no significant increase in the removal. This could be attributed to the fact that at a higher dosage, there is a reduction in the surface area of the adsorbent due to the particle agglomeration (Padmavathy *et al.* 2016). Therefore, the optimum dose of N-ZnO was considered as 2 g/L. Similar findings were reported by various researchers for the removal of SDZ using tea waste biochar, kaolinite etc. and for the removal of AMP using nano-silica adsorbent, coconut shell and activated carbon derived from animal hair (Liu *et al.* 2013; Xu *et al.* 2013; Nam *et al.* 2014; Eslami *et al.* 2020; He *et al.* 2021).

3.2.3. Effect of AMP/SDZ initial concentration

The effect of initial concentration of the target pollutants on the removal was assessed at neutral pH, for an optimum N-ZnO dose and time. Figure 3(c) shows effect of AMP/SDZ initial concentration on removal. From figure, the removal of both the adsorbates was found to decrease with an increase in the initial concentration i.e., as the concentration of AMP and SDZ was increased from 0.5 mg/L to 100 mg/L, the removal was reduced from 70% to 37.45% for SDZ and 70.8% to 16.71% for AMP, respectively. This might be attributed to the fact that, at a higher AMP/SDZ concentration, the active sorption sites found on the surface of the ZnO nanoparticles would have saturated. This results in a reduction in the sorption of AMP/SDZ pollutants onto the adsorbent (Manjunath *et al.* 2020). It can be observed that the rate of reduction is less for SDZ than AMP at lower adsorbate concentrations (0.5 mg/L to 50 mg/L). However, at 5 mg/L adsorbate concentration, the percentage removal remains almost the same (~64%) for both target pollutants.

3.2.4. Effect of pH

The variation of pH was studied at an optimum ZnO nanoparticles dose and at optimum contact time. Effect of pH on removal of AMP and SDZ is depicted in Figure 3(d). From the figure, it can be inferred that the adsorption of AMP and SDZ onto ZnO nanoparticles is a pH-dependent process. A decreasing trend in removal efficiency was observed at a pH greater and less than the neutral range. The $pH_{solution}$ was taken to be 6.8 ± 0.3 throughout experiment. The pK_a value of AMP is 9.3, pK_{a1} and pK_{a2} of SDZ is 1.57 and 6.5, respectively and pH_{pzc} of ZnO nanoparticles is 6.6, respectively. For pHpzc < pHsolution, the adsorbent surface carries negative charge, whereas SDZ and AMP present in solution appear as charged cations (SDZ-H+ and AMP-H+) signifying electrostatic attraction between positively charged ZnO nanoparticles and SDZ-H+ and AMP-H+. However, at higher pH, both adsorbent and adsorbate exist as negatively charged ions. Hence a reduction in removal efficiency at higher pH (10 and 12) is attributed to the repulsion between the like charges (Zyoud *et al.* 2020). AMP/SDZ molecules exist as neutral particles when pH is lower than pK_a. Hence at lower pH (2 and 4), the active sites present on the N-ZnO surface are blocked by the formation of multilayers of contaminants due to strong electrostatic interaction (Basha *et al.* 2015). This results in a reduction in removal percentage at lower pH. However, at neutral pH, the hydrophobic interaction of target pollutants can be considered as the predominant mechanism involved in the adsorption process (Eslami *et al.* 2020). A similar trend was also observed in the removal of SDZ and AMP using other adsorbents such as spent tea leaf generated activated carbon, phosphonic chelating fiber, immobilized laccase, low-cost coconut waste shell, etc. (Ratanapongleka & Punbut 2018; Yanyan *et al.* 2018; Yang *et al.* 2019; Yadav *et al.* 2022).

3.2.5. Effect of temperature

Figure 3(e) represents the variation in removal efficiency with an increase in temperature. The removal of both AMP and SDZ was found to increase with an increase in temperature from 293 to 308 K after a contact time of 30 minutes. The removal efficiency increased from 35.8% to 66% for AMP and 21% to 63% for SDZ. This increase is attributed to the rise in the

diffusion rate of target pollutants to the internal and external pores of the ZnO nanoparticles with an increase in temperature. An increase in temperature is also responsible for increase in the total pore volume and porosity of the sorbent (Banerjee *et al.* 2016).

3.3. Kinetic study

Kinetic models aid in identifying the order and rate of the sorption process. The adsorption of AMP and SDZ onto the N-ZnO surface can be assumed to follow a series of diffusion processes. It starts with film diffusion, where the transfer of adsorbate mass happens from the bulk solution to the adsorbent surface, followed by particle diffusion, which takes place in different forms like pore and surface diffusion (Podder & Majumder 2017). LFD model, EKM and IPD model helps in understanding the diffusion mechanism of AMP and SDZ onto the ZnO nanoparticles surface. Table 3 represents the values of kinetic constants and R^2 (linear regression coefficient) during the adsorption of AMP and SDZ onto the ZnO nanoparticles surface. From Table 3, it can be inferred that with respect to all kinetic models studied, the calculated R^2 value is near to unity for PSO. Also, the equilibrium adsorption capacity calculated using the PSO model (1.82 mg/g and 1.55 mg/g for AMP and SDZ, respectively) was almost similar to the adsorption capacity calculated using the experiment. In LFD, if the plot of $ln(1 - q_e/q_t)$ vs t passes through the origin, implies that the rate-limiting step of adsorption is film diffusion. However, in the LFD model, the curve is nonlinear and the value of A is non-zero. indicating that in the adsorptive removal of AMP and SDZ using N-ZnO nanoparticles, liquid film diffusion is not the only rate-limiting step (Manjunath *et al.* 2019). Similarly, EKM and IPD models were also used to predict if the adsorption mechanism is by pore diffusion. In IPD, the intercept value implies the thickness of the boundary layer (Mall *et al.* 2006). For the removal of both SDZ and AMP, the value of C was found to be high, specifying that the effect of boundary layer is more during adsorption process. In addition, the intercept of the line in IPD and EKM model specifies that pore diffusion solely is not the rate-limiting step in the adsorptive removal of SDZ and AMP by ZnO nanoparticles (Manjunath *et al.* 2019, 2020). Therefore, comparing all kinetic models, the experimental data best fitted PSO model indicating that the sorption of AMP and SDZ onto ZnO nanoparticles is chemisorption.

3.4. Equilibrium study

The isotherm constants for the equilibrium study are shown in Table 4. Comparing the R^2 value of all models it was found that for both SDZ and AMP, LI had a higher R^2 value ($R^2 > 0.98$). This indicates that the monolayer chemisorption happens on the homogeneous sites of ZnO nanoparticles and the adsorption of AMP and SDZ molecules onto one active site of the adsorbent is independent of other molecules present adjacent to it (Kumar *et al.* 2011). The maximum Langmuir adsorption capacity was observed as 7.87 mg/g for AMP and 7.77 mg/g for SDZ. The dimensionless equilibrium or separation factor

Table 3 | Kinetic constants for the adsorption of AMP and SDZ using N-ZnO

Kinetic models	Constants $q_{e,exp}$ (mg/g)	AMP 1.66	SDZ 1.50
Pseudo-first-order	q_e (mg/g)	1.11	0.52
	K_1 (min^{-1})	0.10	0.12
	R^2	0.998	0.919
Pseudo-second-order	q_e (mg/g)	1.82	1.55
	K_2 (g/mg/min)	0.13	0.43
	R^2	0.999	0.999
Liquid-film-diffusion	K_{FD}	0.10	0.12
	A	−0.40	−1.51
	R^2	0.998	0.919
Intra-particle diffusion	C	0.77	1.13
	K_{ID} ($mg/g/min^{0.5}$)	0.14	0.06
	R^2	0.921	0.873
Elovich	α	1.82	330.13
	β	3.30	7.63
	R^2	0.978	0.935

Table 4 | Equilibrium constants for the adsorption of AMP and SDZ using ZnO nanoparticles

Equilibrium models	Constants	AMP	SDZ
Langmuir	q_m	7.87	7.77
	K_L	0.16	0.15
	R^2	0.998	0.988
Freundlich	K_F	0.80	0.87
	n	1.61	1.25
	R^2	0.972	0.986
Temkin	A_T	3.77	6.52
	B	1.42	1.42
	R^2	0.903	0.858
Dubinin-Radushkevich	q_m	4.83	6.68
	K_{DR}	0.14×10^{-6}	0.17×10^{-6}
	R^2	0.829	0.725
Elovich	q_m	4.14	16.00
	K_E	1.05	1.00
	R^2	0.927	0.899

parameter, 'R_L,' (Equation (8)) is used to estimate the favorability of adsorption between the sorbent and the sorbate (Weber & Chakravorti 1974).

$$R_L = \frac{1}{1 + K_L C_o} \tag{8}$$

where, C_o is the concentration of AMP/SDZ molecules at the beginning of the experiment and K_L is the Langmuir constant. Based on the value of R_L, it is possible to anticipate the adsorption nature, i.e. linear adsorption ($R_L > 1$), favorable adsorption ($0 > R_L > 1$) and irreversible adsorption ($R_L < 1$) (Günay *et al.* 2007). From results, the value of R_L was found to be in the range of 0.55 and 0.57 for AMP and SDZ, respectively, indicating that the adsorption process is favorable in nature. On the other hand, FI represents multilayer adsorption and the affinity towards adsorption is determined using ratio 1/n. Adsorption is found to be favorable if the value of 1/n lies between 0 and 1 (Manjunath *et al.* 2019). From Table 4, the value of 1/n was found to be 0.62 and 0.80 for AMP and SDZ, respectively, elucidating that adsorption is favorable in nature. Subsequently, TI is based on the assumption that in a layer, for all the molecules, there is a linear reduction (rather than logarithmic) in the heat of adsorption with respect to the coverage, and subsequently, adsorption is characterized by a uniform distribution of binding energy (Zhang *et al.* 2013). From Table 4, the Temkin adsorption constant A_T was found to be 3.77 L/mmol and 6.52 L/mmol for AMP and SDZ, respectively, and Temkin constant B as 1.42 J/mol for both sorbates. The standard free enthalpy was calculated from Temkin model using Equation (9) (Zhang *et al.* 2013).

$$A_T = \exp\left(\frac{-\Delta G}{RT}\right) \tag{9}$$

where, R and T are universal gas constant (8.314 J/mol K) and absoulte temperature (K), respectively The enthalpy was calculated from Equation (9), which was found to be 3.01 kJ/mol and 4.25 kJ/mol for AMP and SDZ, respectively. Furthermore, the DRI model aims to identify adsorption characteristics on heterogeneous and homogeneous surfaces. Meanwhile, the EI model assumes adsorption to be multilayer based on the presumption that with adsorption, the number of adsorption sites increases exponentially (Hamdaoui & Naffrechoux 2007). However, from the R^2 value obtained from the study, it can be inferred that these two models are ineffective in predicting the adsorption of AMP and SDZ onto the ZnO nanoparticle surface.

3.5. Thermodynamic study

The thermodynamic parameters ΔG^o, ΔS^o, and ΔH^o was determined by performing the adsorption of AMP and SDZ on to ZnO nanoparticles at different temperatures. The result of the study is presented in Table 5. From the study it can be inferred

that, as temperature increased from 293 to 308 K, the value of ΔG^o decreased from 3.11 kJ/mol to 0.08 kJ/mol for AMP and 4.96 kJ/mol to 0.44 kJ/mol for SDZ, respectively. Meanwhile, the positive values of ΔG^o for removal of both AMP and SDZ elucidates that the non-spontaneous nature of the adsorption system and higher temperature enhances the favorability of the adsorption process. (Manjunath *et al.* 2017). The positive value of ΔH^o (64.83 kJ/mol for AMP and 94.43 kJ/mol for SDZ) indicates that the sorption process is endothermic where the process reaches equilibrium by consuming energy from the system considered (Rashtbari *et al.* 2022). The adsorption process in the solid-liquid interface is comprised of two stages, the first stage being the desorption of water molecules (previously adsorbed) from ZnO nanoparticles surface and the sorption of AMP and SDZ species onto the sorbent surface in second stage. For the sorption of AMP and SDZ on the ZnO nanoparticles surface, AMP and SDZ ions have to replace more water molecules which results in endothermic adsorption process. In an endothermic process, the energy is attained from the surrounding environment/molecule in the form of heat. This clearly depicts the adsorption to be chemisorption (Manjunath & Kumar 2018). Furthermore, positive value of ΔS^o (0.211 kJ/mol for AMP and 0.307 kJ/mol for SDZ) implies that a higher translational entropy was found for the displaced water molecules than that of AMP and SDZ ions (Banerjee *et al.* 2016). This causes an increase in randomness at the solid/liquid interface during fixation of AMP and SDZ on active sites of ZnO nanoparticles during the adsorption process (Gaayda *et al.* 2022).

3.6. Competitive adsorption of AMP and SDZ in AMP + SDZ mixture

Competitive Langmuir isotherm model was used to analyze the competitive sorption of SDZ and AMP in MuS. Equations (3) and (4) shows the corresponding Langmuir model for MoS and MuS. In addition, the model's linearized form is represented in Equations (10) and (11). This model helps to explicate the synergistic/antagonistic nature of one sorbate in the presence of another in a MuS (i.e., the effect of AMP on SDZ in AMP + SDZ and the effect of SDZ on AMP in AMP + SDZ).

$$\frac{1}{q_{e,S}} = \frac{1}{Q_{max,S}} + \frac{1}{Q_{max,S} \times K_{L,S}} \left[\frac{1 + K_{L,A} \times C_{e,A}}{C_{e,S}}\right] \tag{10}$$

$$\frac{1}{q_{e,A}} = \frac{1}{Q_{max,A}} + \frac{1}{Q_{max,A} \times K_{L,A}} \left[\frac{1 + K_{L,S} \times C_{e,S}}{C_{e,A}}\right] \tag{11}$$

where, $C_{e,A}$ and $C_{e,S}$ indicate equilibrium concentration of AMP and SDZ, respectively, in AMP + SDZ mixture; $q_{e,A}$ and $q_{e,S}$ represent equilibrium adsorption capacity of AMP and SDZ respectively, in AMP + SDZ mixture; $Q_{max,S}$ and $Q_{max,A}$ depict the capacity of adsorption (maximum) of target pollutants in AMP + SDZ solution and $K_{L,A}$ and $K_{L,S}$ indicate Langmuir constants AMP and SDZ, respectively. The results obtained from the model are presented in Table 6. From table, it can be seen that in MoS, the adsorption capacity of N-ZnO nanoparticle for SDZ was higher when compared to that of AMP. Meanwhile, in a MuS, the adsorption capacity was found to be ~0.88 times and ~1.79 times for AMP and SDZ, respectively in comparison to MoS. In a MuS, the synergistic/antagonistic nature was investigated using the ratio Q_{multi}/Q_{mono}. Where, Q_{mono} and Q_{multi} denotes the adsorption capacity (maximum) of the SDZ and AMP in MoS and MuS. Based on the value of Q_{multi}/Q_{mono}, three possible interactions can be predicted i.e., (a) $Q_{multi}/Q_{mono} = 1$, no interaction, i.e. the sorbates in AMP + SDZ, MuS shows no prominent effect on individual sorbates in the MuS, (b) $Q_{multi}/Q_{mono} < 1$ represents antagonistic

Table 5 | Thermodynamic parameters for the adsorption of AMP and SDZ onto ZnO nanoparticles

Adsorbate	T (K)	ln K_d	ΔG^o (kJ/mol)	ΔH^o (kJ/mol)	ΔS^o (kJ/mol K)	R^2
AMP	293	−1.28	3.11	64.83	0.211	0.93
	298	−0.68	1.68			
	303	−0.11	0.28			
	308	−0.03	0.08			
SDZ	293	−2.04	4.96	94.43	0.307	0.91
	298	−0.97	2.4			
	303	−0.29	0.72			
	308	−0.17	0.44			

Table 6 | Langmuir competitive model for sorption of AMP and SDZ in AMP + SDZ system

System	Adsorbate	Q_m	K_L	Q_{multi}/Q_{single}	R^2
AMP + SDZ	AMP	6.94	0.12	0.88	0.992
	SDZ	13.89	0.04	1.79	0.996

nature, i.e. sorption of one sorbate is lowered by the presence of other in pollutant mixture and (c) $Q_{multi}/Q_{mono} > 1$, represents synergistic interaction, i.e. sorption of one sorbent is enhanced by the presence of other in AMP + SDZ solution.

For AMP, the Q_{multi}/Q_{mono} ratios were found to be less than 1. This indicates an antagonistic effect of AMP in a MuS. i.e., the adsorption of AMP was suppressed in presence of SDZ, indicating a competitive adsorption. However, for SDZ, the Q_{multi}/Q_{mono} ratios were found to be greater than 1. This implies a synergistic effect of SDZ in a MuS. i.e. the adsorption of SDZ was enhanced by the presence AMP in the AMP + SDZ system, indicating a cooperative adsorption. Luo *et al.* 2015; Tovar-Gómez *et al.* 2015; Goze *et al.* 2016; Manjunath *et al.* 2019; Yadav *et al.* 2022, also studied the synergistic/antagonistic nature of different adsorbents and adsorbates in a MuS and reported similar findings.

3.7. Desorption studies

Figure 4 represents the percentage desorption of the target pollutants from the surface of ZnO nanoparticles. During the first cycle, the percentage desorption was found to be 43.03% and 35.6% for AMP and SDZ, respectively. In the second cycle, the desorption was reduced to 31.7% and 24.1% for AMP and SDZ. However, at the end of the third cycle, it was reduced to 25.28% and 22.4% for AMP and SDZ, respectively. It can be inferred that the desorption was higher during the first cycle of adsorption-desorption for both pollutants, which gradually reduced at the end of the third cycle. A lower percentage of desorption indicates a higher affinity of pollutants towards the adsorbent. Hence a strong bond exists between AMP/SDZ and N-ZnO nanoparticle and adsorption is irreversible (Yadav *et al.* 2022).

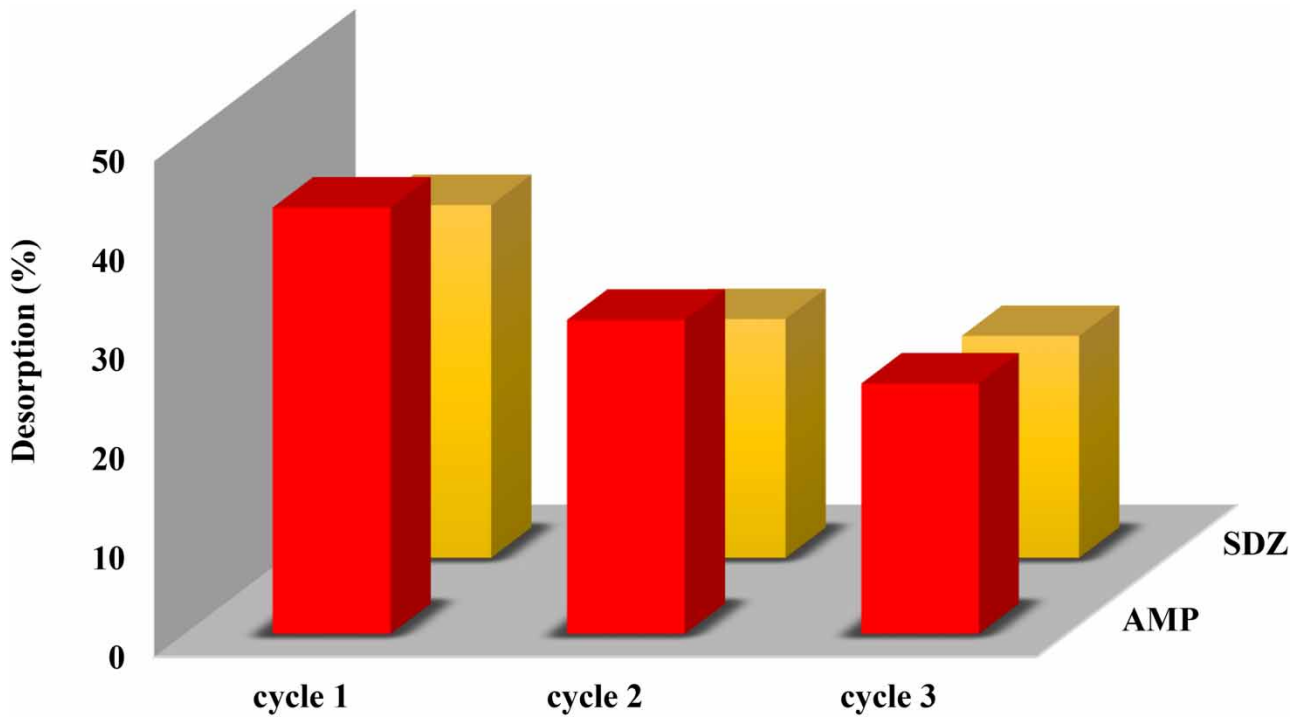

Figure 4 | Desorption of AMP and SDZ from ZnO nanoparticles surface.

3.8. Adsorption mechanism

As observed from the equilibrium study, the removal of AMP and SDZ using ZnO nanoparticles followed the LI model. It indicates that the sorption of both target pollutants on the sorbent is monolayer, and chemisorption is the major mechanism involved in the sorption process. The pore size determined using porosimetry analysis confirms the formation of mesopores (46.843 nm) on the surface of ZnO nanoparticles generated from *A. indica* extract. During the adsorption process, the target pollutants are found to adsorb onto these pores. However, 𝜋-𝜋 interaction, hydrogen bond formation and formation of electron complex are generally considered as the plausible mechanism of AMP adsorption onto sorbent. In the case of SDZ, sulfonamide groups, amino groups, and aromatic rings act as 𝜋 electron acceptors (Peiris *et al.* 2017). Oxygen, in the carbonyl group of AMP molecules, has electron lone pairs acting as acceptors of hydrogen bonds and -OH bond present on the surface of ZnO nanoparticles acts as a donor (Quesada *et al.* 2019). Even though hydrogen bonding is the key mechanism observed in the adsorption of AMP onto the ZnO nanoparticles surface, other interactions like electrostatic forces, covalent bonding and Van der Waals forces are induced between the complex functional groups present on the ZnO nanoparticles surface and AMP molecules (Suriyanon *et al.* 2015). Desorption study also helps to predict the mechanism of adsorption. A lower percentage of desorption in all three cycles indicates the presence of a strong bond (due to chemisorption) between target pollutants and ZnO nanoparticles (Manjunath *et al.* 2019).

Apart from this, the relationship between pH_{pzc} and pH was also used to explain the adsorption mechanism. The pH_{pzc} of ZnO nanoparticles was found to be 6.6. When $pH_{pzc} < pH_{solution}$ the adsorbent surface is negatively charged, whereas SDZ and AMP present in solution occurs as charged cations (SDZ-H^+ and AMP-H^+) signifying electrostatic attraction between positively charged ZnO nanoparticles and SDZ-H^+ and AMP-H^+, respectively. at higher pH, both sorbent and sorbate carry negative charge. Hence a reduction in removal efficiency at higher pH is attributed to the repulsion between the like charges (Zyoud *et al.* 2020). AMP/SDZ molecules exist as neutral particles when pH is lower than pK_a. Hence at lower pH (2 and 4), the active sites present on the ZnO nanoparticles surface are blocked due to the formation of multilayers of contaminants due to strong electrostatic interaction (Basha *et al.* 2015). This results in a reduction in removal percentage at lower pH. However, at neutral pH, the hydrophobic interaction of target pollutants can be considered the predominant mechanism involved in the adsorption process (Eslami *et al.* 2020).

3.9. Performance evaluation of ZnO nanoparticles with other sorbents

The adsorption capacity of ZnO nanoparticles and other adsorbents are compared and represented in Table 7. The maximum adsorption capacity of ZnO nanoparticles used in this study is comparable with other sorbents presented. Whereas the

Table 7 | Operational conditions and adsorption capacity of different adsorbents for the removal of AMP and SDZ

		Operational Conditions					
Adsorbate	Adsorbent	Time (hrs)	C_o (mg/L)	Dose (mg/L)	q_m (mg/g)	Isotherm model	References
SDZ	Expanded graphite	12	5–80	1,000	16.59	LI	Zhang *et al.* (2017)
	High silica ZSM-5	48	0.5–20	200	6.21	FI	Zuo *et al.* (2020)
	Phosphonic chelating cellulos	72	0.3–2	100	0.22	FI	Yang *et al.* (2019)
	Zeolite	1.67	0.5–20	1,000	2.57	LI	Liu *et al.* (2018)
	ZnO nanoparticle (MoS-component)	0.5	0.5–100	2,000	7.77	LI	Present Study
	ZnO nanoparticle (MuS-component)	0.5	1 + 1–100 + 100	2,000	13.89	LI	Present Study
AMP	Amine hexagonal mesoporous silica	10	0.04–0.3	2,000	0.153	LI	Suriyanon *et al.* (2015)
	Mercapto- functionalized hexagonal mesoporous silica	10	0.04–0.3	2,000	0.05	LI	Suriyanon *et al.* (2015)
	Hexagonal mesoporous silica	10	0.04–0.3	2,000	0.03	LI	Suriyanon *et al.* (2015)
	Powdered activated carbon	10	0.04–0.3	2,000	0.50	LI	Suriyanon *et al.* (2015)
	ZnO nanoparticle (MoS-component)	0.5	0.5–100	2,000	7.87	LI	Present Study
	ZnO nanoparticle (MuS-component)	0.5	1 + 1–100 + 100	2,000	6.94	LI	Present Study

removal of both SDZ and AMP from a MuS is not reported by other researchers as seen from literature. The q_m of ZnO nanoparticles in a multi-component system is higher than that of other sorbents in an MoS.

4. CONCLUSION

Synthesis of ZnO nanoparticles were performed using neem (*A. indica*) leaf extract. SEM-EDS, TEM, FTIR, BET and XRD analysis were performed for the characterization of ZnO nanoparticles. ZnO nanoparticles having a surface area of 48.551 m^2/g and an average particle size of 10 nm were obtained at the end of the synthesis. ZnO nanoparticles was found to be effective in removing pharmaceutically active compounds like AMP and SDZ from both MoS and MuS. The equilibrium time, optimum dosage and pH from adsorption study was found to be 30 min, 2 g/L and 7, respectively. The kinetic study best fitted PSO reaction for both AMP and SDZ with an R^2 value nearly unity. The adsorption was monolayer and maximum adsorption capacity was found to be 7.87 mg/g and 7.77 mg/g for AMP and SDZ, respectively. In MuS, from Langmuir competitive model, AMP exhibited antagonistic nature and SDZ exhibited synergistic nature respectively. Percentage desorption obtained for 3 cycles was found to be ~43.03%, ~31.7% and ~25.28% for AMP and ~35.6%, ~24.1% and ~22.4% for SDZ respectively. This lower desorption percentage indicate a stronger bond between the ZnO nanoparticle and AMP/SDZ molecules. From this study it can be concluded that ZnO nanoparticles can be effectively used as a nano-adsorbent for the treatment of pharmaceutically active compounds.

ETHICS APPROVAL AND CONSENT TO PARTICIPATE

Not Applicable.

CONSENT FOR PUBLICATION

Not Applicable.

AVAILABILITY OF DATA AND MATERIALS

Included in the manuscript.

AUTHORS' CONTRIBUTION

All authors contributed to the study's conception and design.
Aswathy Erat Valsan: Supervision and proof reading.
Nayanathara O Sanjeev: Experimentation and Characterization, analysis and manuscript preparation.
Manjunath Singanodi Vallabha: Modeling, Manuscript preparation and proof reading.

FUNDING

Not Applicable.

DATA AVAILABILITY STATEMENT

All relevant data are included in the paper or its Supplementary Information.

CONFLICT OF INTEREST

The authors declare there is no conflict.

REFERENCES

Ahmadzadeh, S. & Dolatabadi, M. 2018 Removal of acetaminophen from hospital wastewater using electro-Fenton process. *Environmental Earth Sciences* **77** (2), 1–11.

Akbour, R. A., El, J., Ezzahra, F., Khenifi, A., Afanga, H., Farahi, A., Yap, P.-S., Forte, M. B. S. & Hamdani, M. 2020 Adsorption of anionic dyes from aqueous solution using polyelectrolyte PDADMAC-modified-montmorillonite clay. *Desalination and Water Treatment* **208**, 407–422.

Ali, K., Dwivedi, S., Azam, A., Saquib, Q., Al-Said, M. S., Alkhedhairy, A. A. & Musarrat, J. 2016 Aloe vera extract functionalized zinc oxide nanoparticles as nanoantibiotics against multi-drug resistant clinical bacterial isolates. *Journal of Colloid and Interface Science* **472**, 145–156.

Ali, E., Islam, M. S., Hossen, M. I., Khatun, M. M. & Islam, M. A. 2021 Extract of neem (Azadirachta indica) leaf exhibits bactericidal effect against multidrug resistant pathogenic bacteria of poultry. *Veterinary Medicine and Science* **7** (5), 1921–1927.

Al Abdullah, K., Awad, S., Zaraket, J. & Salame, C. 2017 Synthesis of ZnO Nanopowders by Using Sol-Gel and Studying Their Structural and Electrical Properties at Different Temperature. *Energy Procedia* **119**, 565–570.

Amouzgar, P., Seng, C. E. & Salamatinia, B. 2017 Effects of ultrasound on development of Cs/NAC nano composite beads through extrusion dripping for acetaminophen removal from aqueous solution. *Journal of Cleaner Production* **165**, 537–551.

Aneesh, P. M., Vanaja, K. A. & Jayaraj, M. K. 2007 Synthesis of ZnO nanoparticles by hydrothermal method. *Nanophototnic Materials IV* **6639**, 1–9.

Angelin, B., Silva, S. & Kannan, S. R. 2015 Zinc Oxide Nanoparticles Impregnated Polymer Hybrids for Efficient Extraction of Heavy Metals From Polluted Aqueous Solution. *Asian Journal of Science and Technology* **6** (12), 2139–2150.

Anusa, R., Ravichandran, C. & Sivakumar, E. K. T. 2017 Removal of heavy metal ions from industrial waste water by nano-ZnO in presence of electrogenerated Fenton' s reagent. *International Journal of ChemTEch Research* **10** (7), 501–508.

Azizi, S., Shahri, M. M. & Mohamad, R. 2017 Green synthesis of zinc oxide nanoparticles for enhanced adsorption of lead Ions from aqueous solutions: Equilibrium, kinetic and thermodynamic studies. *Molecules* **22** (6), 831.

Bala, N., Saha, S., Chakraborty, M., Maiti, M., Das, S., Basu, R. & Nandy, P. 2014 Green synthesis of zinc oxide nanoparticles using Hibiscus subdariffa leaf extract : effect of temperature on synthesis, anti-bacterial activity and anti-diabetic activity. *RSC Advances* **5**, 4993–5003.

Banerjee, P., Das, P., Zaman, A. & Das, P. 2016 Application of graphene oxide nanoplatelets for adsorption of Ibuprofen from aqueous solutions: evaluation of process kinetics and thermodynamics. *Process Safety and Environmental Protection* **101**, 45–53.

Baran, W., Adamek, E., Ziemiańska, J. & Sobczak, A. 2011 Effects of the presence of sulfonamides in the environment and their influence on human health. *Journal of Hazardous Materials* **196**, 1–15.

Basha, S., Keane, D., Nolan, K., Oelgemöller, M., Lawler, J., Tobin, J. M. & Morrissey, A. 2015 UV-induced photocatalytic degradation of aqueous acetaminophen: the role of adsorption and reaction kinetics. *Environmental Science and Pollution Research* **22** (3), 2219–2230.

Bhuyan, T., Mishra, K., Khanuja, M. & Prasad, R. 2015 Biosynthesis of zinc oxide nanoparticles from Azadirachta indica for antibacterial and photocatalytic applications. *Materials Science in Semiconductor Processing* **32**, 55–61.

Briones, R. M., de Luna, M. D. G., Su, C.-C. & Lu, M.-C. 2014 Factors Affecting Fenton Oxidation of Acetaminophen in a Fluidized-Bed Reactor Rowena. *Journal of Environmental Engineering* **140**, 77–83.

Chinnaiyan, P. & Thampi, S. G. 2018 Pharmaceutical products as emerging contaminant in water : relevance for developing nations and identification of critical compounds for Indian environment. *Environmental Monitoring and Assessment* **190** (288), 1–13.

Dayakar, T., Venkateswara Rao, K., Bikshalu, K., Rajendar, V. & Park, S. H. 2017 Novel synthesis and structural analysis of zinc oxide nanoparticles for the non enzymatic glucose biosensor. *Materials Science and Engineering C* **75**, 1472–1479.

Dutta, M., Das, U., Mondal, S., Bhattachriya, S., Khatun, R. & Bagal, R. 2015 Adsorption of acetaminophen by using tea waste derived activated carbon. *International Journal of Environmental Sciences* **6** (2), 270–281.

Elumalai, K. & Velmurugan, S. 2015 Green synthesis, characterization and antimicrobial activities of zinc oxide nanoparticles from the leaf extract of Azadirachta indica (L.). *Applied Surface Science* **345**, 329–336.

Eslami, A., Goodarzvand Chegini, Z., Khashij, M., Mehralian, M. & Hashemi, M. 2020 Removal of acetaminophen (ACT) from aqueous solution by using nanosilica adsorbent: experimental study, kinetic and isotherm modeling. *Pigment and Resin Technology* **49** (1), 55–62.

Gaayda, J. E., Titchou, F. E., Oukhrib, R., Karmal, I., Abou, H., Berisha, A., Zazou, H., Swanson, C., Hamdani, M. & Ait, R. 2022 Removal of cationic dye from coloured water by adsorption onto hematite-humic acid composite: experimental and theoretical studies. *Separation and Purification Technology* **288**.

Ghorbani, H. R., Mehr, F. P., Pazoki, H. & Rahmani, B. M. 2015 Synthesis of ZnO Nanoparticles by Precipitation Method. *Oriental Journal of Chemistry* **31** (2), 1219–1221.

Gomes, I. B., Maillard, J. Y., Simões, L. C. & Simões, M. 2020 Emerging contaminants affect the microbiome of water systems – strategies for their mitigation. *Clean Water* **3** (1), 1–11.

Goze, B., Evirgen, O. A. & Acikel, Y. S. 2016 Investigation of antagonistic and synergistic interactions on simultaneous adsorption of crystal violet and Cu(II) using chitin and chitosan. *Desalination and Water Treatment* **57** (9), 4059–4072.

Günay, A., Arslankaya, E. & Tosun, I. 2007 Lead removal from aqueous solution by natural and pretreated clinoptilolite: adsorption equilibrium and kinetics. *Journal of Hazardous Materials* **146** (1–2), 362–371.

Hamdaoui, O. & Naffrechoux, E. 2007 Modeling of adsorption isotherms of phenol and chlorophenols onto granular activated carbon. Part I. Two-parameter models and equations allowing determination of thermodynamic parameters. *Journal of Hazardous Materials* **147**, 381–394.

Hassan, S. S. M., Abdel-Shafy, H. I. & Mansour, M. S. M. 2016 Removal of pharmaceutical compounds from urine via chemical coagulation by green synthesized ZnO-nanoparticles followed by microfiltration for safe reuse. *Arabian Journal of Chemistry* **12** (8), 4074–4083.

He, X., Li, J., Meng, Q., Guo, Z., Zhang, H. & Liu, Y. 2021 Enhanced adsorption capacity of sulfadiazine on tea waste biochar from aqueous solutions by the two-step sintering method without corrosive activator. *Journal of Environmental Chemical Engineering* **9** (1), 104898.

Kumar, M., Ram, B., Honda, R., Poopipattana, C., Canh, V. D., Chaminda, T. & Furumai, H. 2019 Concurrence of antibiotic resistant bacteria (ARB), viruses, pharmaceuticals and personal care products (PPCPs) in ambient waters of Guwahati, India: Urban vulnerability and resilience perspective. *Science of the Total Environment* **693** (336), 133640.

Kumar, P. S., Ramalingam, S., Kirupha, S. D., Murugesan, A., Vidhyadevi, T. & Sivanesan, S. 2011 Adsorption behavior of nickel(II) onto cashew nut shell: equilibrium, thermodynamics, kinetics, mechanism and process design. *Chemical Engineering Journal* **167** (1), 122–131.

Li, H., Duan, L., Wang, H., Chen, Y., Wang, F. & Zhang, S. 2020 Photolysis of sulfadiazine under UV radiation: Effects of the initial sulfadiazine concentration, pH, NO3− and Cd2+. *Chemical Physics Letters* **739**, 136949.

Liu, H., Ning, W., Cheng, P., Zhang, J., Wang, Y. & Zhang, C. 2013 Evaluation of animal hairs-based activated carbon for sorption of norfloxacin and acetaminophen by comparing with cattail fiber-based activated carbon. *Journal of Analytical and Applied Pyrolysis* **101**, 156–165.

Liu, X., Liu, Y., Lu, S., Guo, W. & Xi, B. 2018 Performance and mechanism into TiO2/Zeolite composites for sulfadiazine adsorption and photodegradation. *Chemical Engineering Journal* **350**, 131–147.

Liu, N., Charrua, A. B., Weng, C. H., Yuan, X. & Ding, F. 2015 Characterization of biochars derived from agriculture wastes and their adsorptive removal of atrazine from aqueous solution: A comparative study. *Bioresource Technology* **198**, 55–62.

Luo, X., Zhang, Z., Zhou, P., Liu, Y., Ma, G. & Lei, Z. 2015 Synergic adsorption of acid blue 80 and heavy metal ions (Cu^{2+}/Ni^{2+}) onto activated carbon and its mechanisms. *Journal of Industrial and Engineering Chemistry* **27**, 164–174.

Madan, H. R., Sharma, S. C., Udayabhanu, Suresh, D., Vidya, Y. S., Nagabhushana, H., Rajanaik, H., Anantharaju, K. S., Prashantha, S. C. & Maiya, P. S. 2015 Facile Green Fabrication of Nanostructure ZnO Plates, Bullets, Flower, Prismatic tip, Closed pine cone: Their Antibacterial, Antioxidant, Photoluminescent and Photocatalytic Properties. *Spectrochimica Acta - Part A: Molecular and Biomolecular Spectroscopy* **152**, 404–416.

Mall, I. D., Srivastava, V. C. & Agarwal, N. K. 2006 Removal of Orange-G and Methyl Violet dyes by adsorption onto bagasse fly ash – kinetic study and equilibrium isotherm analyses. *Dyes and Pigments* **69** (3), 210–223.

Manjunath, S. V. & Kumar, M. 2018 Evaluation of single-component and multi-component adsorption of metronidazole, phosphate and nitrate on activated carbon from Prosopıs julıflora. *Chemical Engineering Journal* **346**, 525–534.

Manjunath, S. V., Baghel, R. S. & Kumar, M. 2019 Performance evaluation of cement–carbon composite for adsorptive removal of acidic and basic dyes from single and multi-component systems. *Environmental Technology and Innovation* **16**, 100478.

Manjunath, S. V., Singh Baghel, R. & Kumar, M. 2020 Antagonistic and synergistic analysis of antibiotic adsorption on Prosopis juliflora activated carbon in multicomponent systems. *Chemical Engineering Journal* **381**, 122713.

Manjunath, S. V., Kumar, S. M., Ngo, H. H. & Guo, W. 2017 Metronidazole removal in powder-activated carbon and concrete-containing graphene adsorption systems: Estimation of kinetic, equilibrium and thermodynamic parameters and optimization of adsorption by a central composite design. *Journal of Environmental Science and Health - Part A Toxic/Hazardous Substances and Environmental Engineering* **52** (14), 1269–1283.

Mankad, M., Patil, G., Patel, S., Pate, D. & Patel, A. 2016 Green synthesis of zinc oxide nanoparticles using Azadirachta indica A . *Juss* . *leaves extract and its antibacterial activity against Xanthomonas orzyae pv. oryzae* **5** (2), 76–86.

Moritz, M. & Geszke-Moritz, M. 2013 The newest achievements in synthesis, immobilization and practical applications of antibacterial nanoparticles. *Chemical Engineering Journal* **228**, 596–613.

Matinise, N., Fuku, X. G., Kaviyarasu, K., Mayedwa, N. & Maaza, M. 2017 Applied Surface Science ZnO nanoparticles via Moringa oleifera green synthesis : Physical properties & mechanism of formation. *Applied Surface Science* **406**, 339–347.

Moussavi, G., Hossaini, Z. & Pourakbar, M. 2016 High-rate adsorption of acetaminophen from the contaminated water onto double-oxidized graphene oxide. *Chemical Engineering Journal* **287**, 665–673.

Moustafa Ahmed P, N. P. & Yousef, N. P. 2015 Synthesis and Characterization of Zinc Oxide Nanoparticles for the removal of CrVI. *International Journal of Scientific & Engineering Research* **6** (7), 1235–1243.

Mutiyar, P. K., Kumar, S. & Kumar, A. 2018 Fate of pharmaceutical active compounds (PhACs) from river Yamuna , India : An ecotoxicological risk assessment approach. *Ecotoxicology and Environmental Safety* **150**, 297–304.

Nam, S. W., Choi, D. J., Kim, S. K., Her, N. & Zoh, K. D. 2014 Adsorption characteristics of selected hydrophilic and hydrophobic micropollutants in water using activated carbon. *Journal of Hazardous Materials* **270**, 144–152.

Natarajan, R., Banerjee, K., Kumar, P. S., Somanna, T., Tannani, D., Arvind, V., Raj, R. I., Vo, D. V. N., Saikia, K. & Vaidyanathan, V. K. 2021 Performance study on adsorptive removal of acetaminophen from wastewater using silica microspheres: Kinetic and isotherm studies. *Chemosphere* **272**, 129896.

Nayak, A., Sahoo, J. K., Sahoo, S. K. & Sahu, D. 2020 Removal of Congo red dye from aqueous solution using zinc oxide nanoparticles synthesised from Ocimum sanctum (Tulsi leaf): a green approach. *International Journal of Environmental Analytical Chemistry*, 1–22.

Padmavathy, K. S., Madhu, G. & Haseena, P. V. 2016 A study on effects of pH, adsorbent dosage, time, initial concentration and adsorption isotherm study for the removal of hexavalent chromium (Cr (VI)) from wastewater by magnetite nanoparticles. *Procedia Technology* **24**, 585–594.

Pai, S., S, H., Varadavenkatesan, T., Vinayagam, R. & Selvaraj, R. 2019 Photocatalytic zinc oxide nanoparticles synthesis using Peltophorum pterocarpum leaf extract and their characterization. *Optik* **185**, 248–255.

Pandimurugan, R. & Thambidurai, S. 2016 Novel seaweed capped ZnO nanoparticles for effective dye photodegradation and antibacterial activity. *Advanced Powder Technology* **27** (4), 1062–1072.

Pandey, G., Verma, K. & Singh, M. 2014 Evaluation of phytochemical, antibacterial and free radical scavenging properties of Azadirachta indica (neem) leaves. *International Journal of Pharmacy and Pharmaceutical Sciences* **6** (2), 444–447.

Peiris, C., Gunatilake, S. R., Mlsna, T. E., Mohan, D. & Vithanage, M. 2017 Biochar based removal of antibiotic sulfonamides and tetracyclines in aquatic environments: a critical review. *Bioresource Technology* **246**, 150–159.

Phong Vo, H. N., Le, G. K., Hong Nguyen, T. M., Bui, X. T., Nguyen, K. H., Rene, E. R., Vo, T. D. H., Thanh Cao, N. D. & Mohan, R. 2019 Acetaminophen micropollutant: Historical and current occurrences, toxicity, removal strategies and transformation pathways in different environments. *Chemosphere* **236**, 124391.

Podder, M. S. & Majumder, C. B. 2017 Biosorption of As(III) and As(V) on the surface of TW/MnFe2O4 composite from wastewater: kinetics, mechanistic and thermodynamics. *Applied Water Science* **7** (6), 2689–2715.

Quesada, H. B., Cusioli, L. F., de O Bezerra, C., Baptista, A. T. A., Nishi, L., Gomes, R. G. & Bergamasco, R. 2019 Acetaminophen adsorption using a low-cost adsorbent prepared from modified residues of Moringa oleifera Lam. seed husks. *Journal of Chemical Technology and Biotechnology* **94** (10), 3147–3157.

Rashtbari, Y., Afshin, S., Hamzezadeh, A., Gholizadeh, A., Ansari, F. J., Poureshgh, Y. & Fazlzadeh, M. 2022 Green synthesis of zinc oxide nanoparticles loaded on activated carbon prepared from walnut peel extract for the removal of Eosin Y and Erythrosine B dyes from aqueous solution: experimental approaches, kinetics models, and thermodynamic studies. *Environmental Science and Pollution Research* **29** (4), 5194–5206.

Ratanapongleka, K. & Punbut, S. 2018 Removal of acetaminophen in water by laccase immobilized in barium alginate. *Environmental Technology* **39** (3), 336–345.

Rathi, B. S. & Kumar, P. S. 2021 Application of adsorption process for effective removal of emerging contaminants from water and wastewater. *Environmental Pollution* **280**, 116995.

Sahito, S. R., Memon, M. A., Kazi, T. G., Kazi, G. H., Jakhrani, M. A., Haque, Q. U. & Shar, G. Q. 2003 Evaluation of mineral contents in medicinal plant Azadirachta indica (Neem). *Journal of the Chemical Society of Pakistan* **25** (2), 139–143.

Sangeetha, G., Rajeshwari, S. & Venckatesh, R. 2011 Green synthesis of zinc oxide nanoparticles by aloe barbadensis miller leaf extract : Structure and optical properties. *Materials Research Bulletin* **46** (12), 2560–2566.

Saranya, N., Ajmani, A., Sivasubramanian, V. & Selvaraju, N. 2018 Hexavalent chromium removal from simulated and real effluents using Artocarpus heterophyllus peel biosorbent – batch and continuous studies. *Journal of Molecular Liquids* **265**, 779–790.

Sim, W. J., Lee, J. W., Lee, E. S., Shin, S. K., Hwang, S. R. & Oh, J. E. 2011 Occurrence and distribution of pharmaceuticals in wastewater from households, livestock farms, hospitals and pharmaceutical manufactures. *Chemosphere* **82** (2), 179–186.

Soliman, M. M. A., Alegria, E. C. B. A., Ribeiro, A. P. C., Alves, M. M., Saraiva, M. S., Fátima Montemor, M. & Pombeiro, A. J. L. 2020 Green synthesis of zinc oxide particles with apple-derived compounds and their application as catalysts in the transesterification of methyl benzoates. *Dalton Transactions* **49** (19), 6488–6494.

Subedi, B., Balakrishna, K., Joshua, D. I. & Kannan, K. 2017 Mass loading and removal of pharmaceuticals and personal care products including psychoactives, antihypertensives, and antibiotics in two sewage treatment plants in southern India. *Chemosphere* **167**, 429–437.

Suriyanon, N., Permrungruang, J., Kaosaiphun, J., Wongrueng, A., Ngamcharussrivichai, C. & Punyapalakul, P. 2015 Selective adsorption mechanisms of antilipidemic and non-steroidal anti-inflammatory drug residues on functionalized silica-based porous materials in a mixed solute. *Chemosphere* **136**, 222–231.

Taheran, M., Naghdi, M., Brar, S. K., Verma, M. & Surampalli, R. Y. 2018 Emerging contaminants: here today, there tomorrow. *Environmental Nanotechnology, Monitoring and Management* **10**, 122–126.

Thomaidis, N. S., Asimakopoulos, A. G. & Bletsou, A. A. 2012 Emerging contaminants: a tutorial mini-review. *Global Nest Journal* **14** (1), 72–79.

Titchou, F. E., Akbour, R. A., Assabbane, A. & Hamdani, M. 2020 Groundwater for sustainable development removal of cationic dye from aqueous solution using Moroccan pozzolana as adsorbent : isotherms, kinetic studies, and application on real textile wastewater treatment. *Groundwater for Sustainable Development* **11**, 100405.

Titchou, F. E., Zazou, H., Afanga, H., Gaayda, J. E. & Akbour, R. A. 2021 Groundwater for sustainable development removal of Persistent Organic Pollutants (POPs) from water and wastewater by adsorption and electrocoagulation process. *Groundwater for Sustainable Development* **13**, 100575.

Tovar-Gómez, R., Moreno-Virgen, M. d. R., Moreno-Pérez, J., Bonilla-Petriciolet, A., Hernández-Montoya, V. & Durán-Valle, C. J. 2015 Analysis of synergistic and antagonistic adsorption of heavy metals and acid blue 25 on activated carbon from ternary systems. *Chemical Engineering Research and Design* **93**, 755–772.

Varadavenkatesan, T., Lyubchik, E., Pai, S., Pugazhendhi, A., Vinayagam, R. & Selvaraj, R. 2019 Photocatalytic degradation of Rhodamine B by zinc oxide nanoparticles synthesized using the leaf extract of Cyanometra ramiflora. *Journal of Photochemistry & Photobiology, B: Biology* **199**, 111621.

Vinayagam, R., Selvaraj, R., Arivalagan, P. & Varadavenkatesan, T. 2020 Synthesis, characterization and photocatalytic dye degradation capability of Calliandra haematocephala-mediated zinc oxide nanoflowers. *Journal of Photochemistry and Photobiology B: Biology* **203**, 111760.

Vinayagam, R., Pai, S., Murugesan, G., Varadavenkatesan, T. & Selvaraj, R. 2021 Synthesis of photocatalytic zinc oxide nanoflowers using Peltophorum pterocarpum pod extract and their characterization. *Applied Nanoscience*, 1–11.

Wang, H., Yuan, X., Wu, Y., Huang, H., Zeng, G., Liu, Y., Wang, X., Lin, N. & Qi, Y. 2013 Adsorption characteristics and behaviors of graphene oxide for Zn(II) removal from aqueous solution. *Applied Surface Science* **279**, 432–440.

Weber, T. W. & Chakravorti, R. K. 1974 Pore and solid diffusion models for fixed-bed adsorbers. *AIChE Journal* **20** (2), 228–238.

Wong, S., Lim, Y., Ngadi, N. & Mat, R. 2018 Removal of acetaminophen by activated carbon synthesized from spent tea leaves: equilibrium, kinetics and thermodynamics studies. *Powder Technology* **338**, 878–886.

Xu, J., He, Y., Zhang, Y., Guo, C., Li, L. & Wang, Y. 2013 Removal of sulfadiazine from aqueous solution on kaolinite. *Frontiers of Environmental Science and Engineering* **7** (6), 836–843.

Yadav, M. S. P., Sanjeev, N. O., Vallabha, M. S., Sekar, A., Valsan, A. E. & Varghese, G. K. 2022 Competitive adsorption analysis of antibiotics removal from multi-component systems using chemically activated spent tea waste: effect of operational parameters, kinetics, and equilibrium study. *Environmental Science and Pollution Research*, 1–16.

Yang, J. F., He, M., Wu, T. F., Hao, A. P., Zhang, S. B., Chen, Y. D., Zhou, S. B., Zhen, L. Y., Wang, R., Yuan, Z. L. & Deng, L. 2018 Sulfadiazine oxidation by permanganate: Kinetics, mechanistic investigation and toxicity evaluation. *Chemical Engineering Journal* **349**, 56–65.

Yang, Y., Zheng, L., Zhang, T., Yu, H., Zhan, Y., Yang, Y., Zeng, H., Chen, S. & Peng, D. 2019 Adsorption behavior and mechanism of sulfonamides on phosphonic chelating cellulose under different pH effects. *Bioresource Technology* **288**, 121510.

Yanyan, L., Kurniawan, T. A., Zhu, M., Ouyang, T., Avtar, R., Dzarfan Othman, M. H., Mohammad, B. T. & Albadarin, A. B. 2018 Removal of Acetaminophen from synthetic wastewater in a fixed-bed column adsorption using low-cost coconut shell waste pretreated with NaOH, HNO3, ozone, and/or chitosan. *Journal of Environmental Management* **226**, 365–376.

Yuvaraja, G., Prasad, C., Vijaya, Y. & Subbaiah, M. V. 2018 Application of ZnO nanorods as an adsorbent material for the removal of As(III) from aqueous solution: kinetics, isotherms and thermodynamic studies. *International Journal of Industrial Chemistry* **9** (1), 17–25.

Zhang, F., Lan, J., Yang, Y., Wei, T., Tan, R. & Song, W. 2013 Adsorption behavior and mechanism of methyl blue on zinc oxide nanoparticles. *Journal of Nanoparticle Research* **15** (11), 1–10.

Zhang, L., Wang, Y., Jin, S. W., Lu, Q. Z. & Ji, J. 2017 Adsorption isotherm, kinetic and mechanism of expanded graphite for sulfadiazine antibiotics removal from aqueous solutions. *Environmental Technology* **38** (20), 2629–2638.

Zuo, X., Qian, C., Ma, S. & Xiong, J. 2020 Sulfonamide antibiotics sorption by high silica ZSM-5: effect of pH and humic monomers (vanillin and caffeic acid). *Chemosphere* **248**, 126061.

Zyoud, A. H., Zubi, A., Hejjawi, S., Zyoud, S. H., Helal, M. H., Zyoud, S. H., Qamhieh, N., Hajamohideen, A. R. & Hilal, H. S. 2020 Removal of acetaminophen from water by simulated solar light photodegradation with ZnO and TiO2 nanoparticles: catalytic efficiency assessment for future prospects. *Journal of Environmental Chemical Engineering* **8** (4), 104038.

First received 1 October 2022; accepted in revised form 18 December 2022. Available online 27 December 2022